Growth conditions, stoichiometry, and electronic structure of lattice-matched SrO/BaO mixtures on Si(100)

J. Zachariae and H. Pfnür*

Institut für Festkörperphysik, Universität Hannover, Appelstrasse 2, D-30167 Hannover, Germany

(Received 1 March 2005; published 3 August 2005)

The low temperature growth conditions of mixed $Ba_{0.7}Sr_{0.3}O$ layers on Si(100) were investigated using the combination of low energy electron diffraction, x-ray photoemission (XPS), and electron energy loss spectroscopy. With these methods crystallinity, stoichiometry, and electronic structure of both occupied and unoccupied levels were studied as a function of layer thickness. Oxide layers were generated by evaporating the metals in oxygen ambient pressure with the sample at room temperature after determination of the minimum oxygen pressure necessary for full oxidation. Good crystallinity with perfect lattice matching was only obtained starting with preadsorbed metallic layers at a concentration close to one monolayer (ML), with best results starting from the $Sr(5 \times 1)$. The XPS analysis shows that a sharp interface is formed during oxidation. The chemical species present at the interface are up to 1 ML of mono-oxidized Si and 1 ML of a mixed Sr–O–Si species. No silicide and silicate species or SiO_2 formation at the interface after oxidation were found. Both interface and mixed oxide layers turned out to be stable to temperatures up to at least 600 °C. Starting already at 1 ML of $Ba_{0.7}Sr_{0.3}O$, the band gap was found to be 4.3 eV, independent of layer thickness. We determined the valence band offset with respect to *n*-Si to be −2.2 eV, resulting in a conduction band offset of +1.0 eV.

I. INTRODUCTION

During the ongoing process of miniaturization of electronic circuits the oxide thickness in conventional complementary metal-oxide-semiconductor (CMOS) technology has now reached the limit of about 2 nm using SiO_2, which already causes high leakage currents in CMOS transistors. As a consequence, an intensive search for alternatives to SiO_2 as a gate dielectric with higher dielectric constant, *K*, started in recent years. This search has concentrated in the past mainly on binary,[1] but partly also on ternary oxides like the titanates of Ba and Sr.[2] Currently HfO_2 and ZrO_2 seem to be the favorites for the first generation of high-*K* oxides to replace SiO_2 in fabrication. They still have the disadvantage of formation of a thin SiO_2 interfacial layer so that no direct interface with Si is formed.

No attempt is currently made to introduce crystalline growth into fabrication, which could potentially further reduce the concentration of defects below the level of amorphous or polycrystalline material by perfect crystalline and stoichiometric growth.

Both disadvantages, small *K* and noncrystalline growth, can be overcome by use of the oxides of Ba and Sr.[1] Here the advantage of miscibility can directly be used to obtain a perfect lattice match, and the formation of an abrupt interface formation has been already demonstrated.[2] Extensive studies have been carried out for $BaTiO_3$ and $SrTiO_3$ as well as for mixed $Sr_xBa_{1-x}O_3$ layers on Si(100).[2–9] These layers were typically grown at elevated temperatures. The growth process was interpreted to start with the formation of a metal silicide layer, which was considered to stabilize the interface and to be not only a necessary precondition for epitaxial growth of the oxides,[7–9] but also to be a stable chemical species that is inert to subsequent the oxidation process. These assumptions have recently been questioned by theoret-

ical studies investigating the atomic structure at the $Si—SrTiO_3$ and $Si—Sr$ interfaces.[10,11] They show that the energetically most favorable structures of interfaces between Si and the oxide are in fact atomically sharp and restricted to the combination of the topmost Si layer and one layer strontium oxide. Interfaces without oxygen, 1 ML, and 1.5 ML of oxygen were investigated. Up to 1 ML is only coordinated with Si forming mono-oxidized Si, whereas the rest forms mixed $Sr—O—Si$ bonds, but no configurations were found that resemble typical metal silicide or silicate coordinations.

These contradicting predictions can best be clarified using a low temperature process during oxidation, as suggested recently by Lettieri *et al.*,[12] so that a presumably existing silicide would more easily survive than with the high temperature process. This process also starts with an Sr layer deposited and ordered around 700°, whereas further metal deposition and oxidation in order to form $Ba_{0.7}Sr_{0.3}O$ was carried out not far from room temperature. This was also the approach we used here.

In our study presented here, we extend significantly these previous investigations of the $Ba_{0.7}Sr_{0.3}O$ system on Si(100) by combining structural information, obtained with low energy electron diffraction (LEED), and electronic information using both core level spectroscopy (XPS) and electron energy loss spectroscopy (EELS). Thus we are able to determine optimal growth conditions as well as the chemical species at the interface and to correlate the amount of oxygen at the interface with optimal growth. The combination of XPS and EELS also allowed the determination of band gaps and band alignment. As we will show below, no silicides exist under our preparation conditions whatsoever. But even more important, this combination of LEED with XPS and EELS also allowed the calibration of concentrations for the different oxygen species at the interface. Thus this study can serve as a basis for the elaboration of how to adjust the band align-

ment by controlled insertion of various oxidic species at the interface.[10] The static dielectric constants of $Ba_{0.7}Sr_{0.3}O$ should be in range of 30 due to the static dielectric constants of 13.3 for SrO and 34 for BaO.[13]

II. EXPERIMENT

All experiments were carried out in an ultrahigh vacuum system at a base pressure of 1×10^{-10} mbar after bakeout. This system was equipped with a hemispherical electron energy analyzer and an Al/Mg twin anode for x-ray photoemission spectroscopy (XPS). Mg $K\alpha$ radiation and a normal emission geometry were used for all measurements. Our XPS spectrometer was calibrated to the $Au4f_{7/2}$ peak position at 84.00 ± 0.05 eV below the Fermi-edge inflection point. An electron gun with an extra concentric hemispherical analyzer is used for electron energy loss spectroscopy (EELS). High resolution low energy electron diffraction (SPA-LEED) is used to control and characterize the morphology of the surface. With this spot profile analysis-LEED it is possible to measure high resolution line scans through the diffraction pattern. A retractable quartz crystal microbalance (QCM) is used to measure *in situ* the mass flux at the position of the sample and to perform the oxidation experiment.

The sample, $14 \times 14 \times 0.5$ mm in size, was a (001) orientated n-type Si single crystal, doped with phosphorus at a concentration of 2×10^{15} cm^{-3} (conductivity of $3-5$ Ω cm at room temperature). After chemical cleaning the sample was transferred into vacuum and degassed at 600 °C for 12 h. In order to remove the chemical silicon oxide the sample was rapidly heated to 950 °C. After this procedure LEED measurements showed the typical (2×1) reconstruction of the clean Si(001)-surface without oxidic species. Also other impurities were below the detection limit of XPS. Substrate temperatures were measured by an infrared pyrometer.

The alkaline earth metals strontium and barium were deposited onto the silicon substrate by electron-beam evaporation from titanium crucibles, monitored by additional quartz microbalances. A constant deposition rate was achieved by regulating the heating power and monitoring the ion flux.

For oxidation molecular oxygen (99.998% purity) was introduced into the chamber by backfilling it to the desired pressure, avoiding any direct gas flow from the gas inlet to the sample. Pressures were measured using a well degassed extractor gauge.

III. RESULTS

A. Growth of lattice matched SrO/BaO oxide films

As mentioned, the quality of epitaxial growth depends on the exact composition of the layer, but it depends also strongly on the starting surface. We found it to be absolutely necessary to start oxide growth with predeposition of about 1 ML of Ba or Sr. Growth without one of these intermediate layers leads only to amorphous oxide layers. On these intermediate layers even a pure SrO layer can be grown epitaxially on the Si(100) surface, although with a lot of dislocations in it. In this paper we concentrate on the composition

$Sr_xBa_{1-x}O$ with $x = 0.3$. We first describe various possibilities of intermediate starting layers that can be used for epitaxial growth after having prepared a clean Si(100) sample as described above, and then show the quality of mixed oxide layers that have been obtained. Adjustment of the composition is carried out using quartz microbalances (see Sec. III A 2), the precision of having reached the exact mixture has to be judged by the quality of the epitaxial layer in LEED and elements concentration obtained by XPS.

1. Intermediate layer

All intermediate layers are grown by the deposition of one of the alkaline earth metals barium or strontium. Intermediate layers on which we were able to grow epitaxial $Sr_{0.3}Ba_{0.7}O$ were Sr layers with coverages of 1, 1.2, and 1.33 ML. They show (2×1), (5×1), and (3×1) reconstructions, respectively.[11,14] Also the (4×1) reconstruction of 1 ML of barium[15] turned out to be suitable.

Optimal ordering of these layers was only obtained at elevated substrate temperatures, for the $Sr(2 \times 1)$ at 700 °C, for the $Sr(5 \times 1)$ at 650 °C, for the $Sr(3 \times 1)$ at 600 °C, and for the $Ba(4 \times 2)$ at 800 °C. Outside this small coverage range between 1 and 1.33 ML the quality of epitaxial growth rapidly deteriorated, and in general only amorphous layers could be grown. Most of the results detailed below were grown on the $Sr(5 \times 1)$ intermediate layer. This layer can be produced in a very well ordered form, as demonstrated in Fig. 1. It is likely that this phase consists of a regular array of domain walls in order to accommodate the high concentration of Sr atoms on the surface and at the same time allow site specific adsorption for the majority of Sr atoms. A schematic is shown in the lower part of Fig. 1.

2. Optimization of the oxide layers

Two methods were tested to deposit SrO an BaO onto the silicon substrate. The first method is evaporate BaO and SrO without excess oxygen. This procedure was not successful, since it produced only amorphous layers, independent of the kind of intermediate layer. Two main reasons may be responsible: First, these oxides evaporate at temperatures in the range of 1000–1200 C,[17] i.e., a small percentage is already dissociated and growth of slightly understoichiometric layers is likely. The main reason, however, most likely was that especially BaO always contained some fraction of hydroxide after preparation of the evaporator, which coevaporates, so that the direct deposition of BaO and SrO molecules always leads to amorphous mixtures consisting of both oxide and hydroxide.

The successful strategy was to evaporate Ba and Sr metal atoms onto the Si(100) surface, and to oxidize them simultaneously in an ambient oxygen pressure, after having deposited the intermediate layers described above.

Alkali earth metals like Ba and Sr in combination with elevated temperatures and excess oxygen may promote the formation SiO_2 at the interface.[18–21] Such unwanted interface layers also restrict the quality of epitaxial oxide growth. Therefore the growth takes place at room temperature and the oxygen pressure must be well controlled, depending on
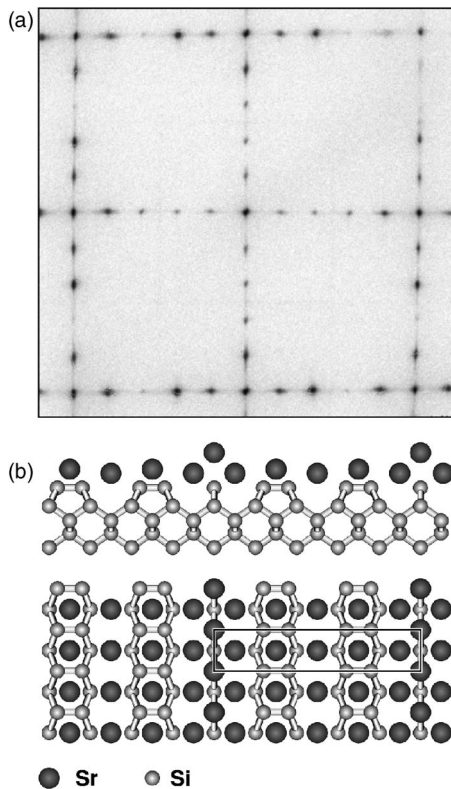
FIG. 1. (a) LEED-pattern after adsorption of 1.2 ML Sr on Si(001) showing a (5×1) reconstruction. (b) Real space model adapted from the 1.33 ML (3×1) structure (Refs. 11 and 16).

the deposition rates of the metals. Following the procedure suggested in Ref. 12, we determined the minimum pressure necessary for complete oxidation of both Ba and Sr at a given evaporation rate by mass accumulation onto the QCM.

The correct fraction between the pure Sr and Ba fluxes is controlled directly by the QCM at the sample and held constant by monitoring the ion current at the evaporators. The evaporators were adjusted to a ratio of the *atom flux* of 7:3 for barium to strontium. In order to adjust the optimal oxygen pressure for complete oxidation of the Sr and Ba layers, the increased mass accumulation during oxidation compared with evaporation of the metallic layers without oxygen on the QCM at the sample position is used. Similar to the procedure described in Ref. 12, the oxygen pressure was increased until the rate or mass accumulation did not change any more by a further increase of oxygen pressure. The oxidation of barium seems to have a catalytic effect on the strontium oxidation. Therefore the pressure, first calibrated with oxidation of pure Sr, had to be lowered by roughly a factor to 2 in the presence of Ba. At our typical evaporation rates of 2 ML per minute, an oxygen pressure of 6×10^{-8} mbar was sufficient for complete oxidation of the metals. As seen from the spectroscopic data presented below, we were thus able to competely avoid the formation of silicon oxides apart from that directly in contact with the interface.

3. Growth and crystallinity of mixed $Sr_{0.3}Ba_{0.7}O$ layers

Crystalline growth can indeed be achieved by fine-tuning the ratio of Ba to Sr evaporation and keeping it constant

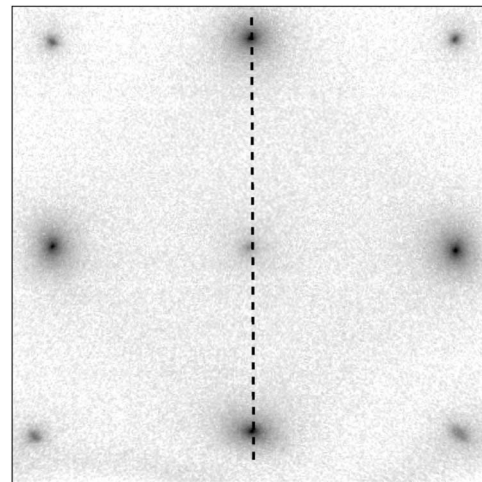FIG. 2. LEED pattern of a 62 ML thick $Ba_{0.7}Sr_{0.3}O$ layer, demonstrating crystalline and epitaxial growth of the oxide layer with 0° orientation relative to the Si(100) substrate. Intensities are plotted on a log scale. Line scans plotted in Fig. 3 are taken along the dashed line.

during the whole procedure. The indication is the match of lattice constants, especially for thicker layers above 10 ML, as determined from the positions of the diffraction spots with the SPA-LEED instrument. A representative example of the diffraction pattern obtained after deposition of about 17 nm (62 ML) of mixed $Ba_{0.7}Sr_{0.3}O$ layers is shown in Fig. 2.

More details of the growth close to the interface as much as for thick layers are revealed by line scans at 51 eV through the diffraction spot profiles, which have been performed along the dashed line shown in Fig. 2. Their evolution as a function of layer thickness is shown in a few characteristic examples in Fig. 3: Starting at line scan (a) with a clean (2×1) reconstructed Si(001) surface. After evaporation of 1.2 ML Sr at 600 °C the $Sr(5 \times 1)$ reconstruction appears in line scan (b). A profile measured after metallic deposition of Ba and Sr in oxygen atmosphere at the rates and pressure settings given above, leading to approximately 1 ML of $Ba_{0.7}Sr_{0.3}O$, is shown in profile (c) in Fig. 3. It reveals the coexistence of several structures at various oxidation states. The presence of a remaining (5×1) structure indicates that there are unoxidized patches of metallic Sr left from the predeposited Sr layer. It quickly disappears by further oxidation, as tested, but it is evident that the oxide layer at this low coverage is not completely closed yet. This finding may be indicative for the formation of a double layer as a first oxidic layer, as found in other systems of insulator growth,[22] but no detailed investigations were carried out at this stage. These patches coexist with a (2×1) structure. This structure is best developed when a pure Sr layer is oxidized, e.g., by the oxidation of the Sr (3×2) phase at one-third monolayer coverage (see also Sec. III C). The (2×1) structure is also seen when higher Sr coverages are oxidized. This structure cannot be due to the previous (2×1) structure of the clean Si(001) surface. It is characteristic of a Sr−O−Si interface, as will be shown later in Sec. III C. Also from the spectroscopic data described below, a formation of such an interface layer seems to be more likely under our growth
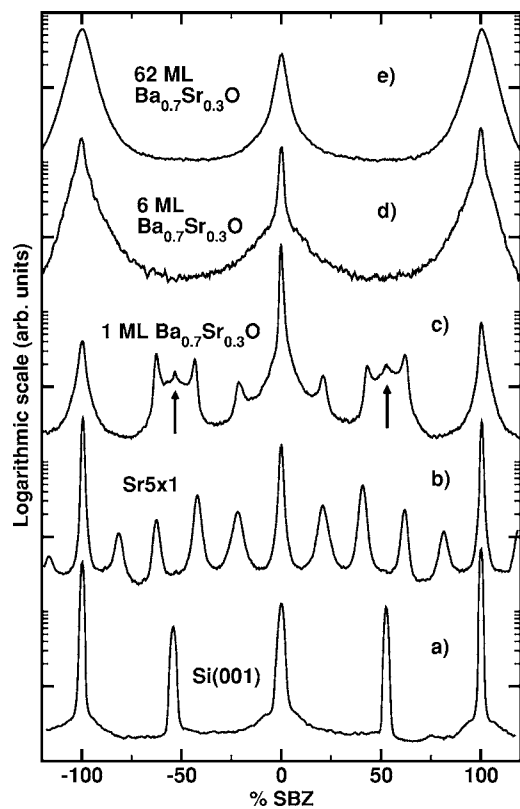
FIG. 3. SPA-LEED line scans at various stages of oxide growth, taken at 51 eV. Scans are taken along the dashed line marked in Fig. 2. (a) pure Si(100)-(2×1) structure. (b) (5×1) structure of 1.2 ML Sr. (c) Initial growth of $Ba_{0.7}Sr_{0.3}O$ on top of the Sr layer (for details, see text). A mixture of (2×1), (5×1), and (1×1) structures is seen. (d) and (e) (1×1) structures characteristic for thicker $Ba_{0.7}Sr_{0.3}O$ layers.

conditions than the formation of a silicide layer.[8,9] As will be detailed in Sec. III B, the latter can clearly be ruled out. For a thicker $Ba_{0.7}Sr_{0.3}O$ layer only the (1×1) alignment of the lattice matched oxide remains, as seen in the line scans (d) and (e) in Fig. 3. The position of the first order spots at ±100% SBZ (surface Brillouin zone) of the Si(001) surface reflect the correct mixture between SrO and BaO. The thick $Sr_{0.3}Ba_{0.7}O$ layer shows broader diffraction spots compared to the Si(001) surface or the Sr(5×1) intermediate layer, see, e.g., line scan (e) in Fig. 3. The reason this broadening is not necessarily an increase of roughness.[23]

B. Electronic structure of $Sr_{0.3}Ba_{0.7}O$ layers

1. The oxide interface

In order to characterize the interface, and the approximate width of the interface, we carried out XPS measurements using Mg $K\alpha$ radiation. Both the Si 2p (see Fig. 4) and O 1s spectra (Fig. 6) as a function of layer thickness were investigated in detail. It turned out that a unique identification of the state of oxidation of the Si surface is complicated by an overlap with characteristic satellite peaks of the Ba $4d_{5/2}$ and $4d_{3/2}$ emissions seen in pure or mixed barium oxide. As shown in Fig. 5, these satellite peaks are shifted by 9.7 eV
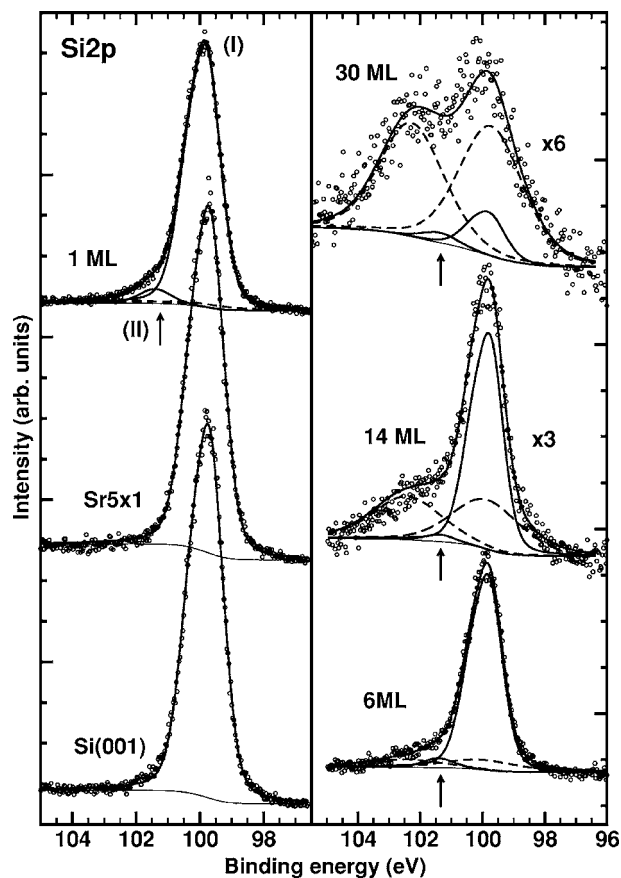

FIG. 4. Evolution of the Si 2p peak during oxide growth. Left: clean Si(001) surface (bottom), after adsorption of 1.2 ML of Sr (middle) and with 1 ML of $Sr_{0.3}Ba_{0.7}O$. The small shoulder of the Si 2p peak in this spectrum at 101.4 eV binding energy is due to the oxide at the interface. Right: Thicker oxide layers, as indicated. The satellite peaks of the Ba 4d emission are solely responsible for the shoulder appearing at the damped Si 2p peaks, and are not due to oxidation of the Si interface, as demonstrated in Fig. 7.

with respect to the main emission peaks, irrespective of the underlying substrate. They exist only in the oxide, not in a metallic Ba layer. An XPS spectrum of a 20 nm thick amorphous $Ba_{0.7}Sr_{0.3}O$ layer evaporated onto Ta demonstrates the independence of these satellite peaks from the substrate, as shown in the spectrum (b) of Fig. 5. Ratio, shape, and position of these satellite peaks are almost identical for an amorphous layer on Ta and a 62 ML thick crystalline oxide layer on Si(001), where the substrate signal is damped to zero. While the origin of these satellite peaks has not been uniquely identified yet—they do not correspond to a typical excitation across the band gap, but may be due to emission of an additional valence electron—it is obvious that the overlap with part of the Si 2p spectrum can easily lead to misinterpretations of these spectra in terms of the oxidation state of the Si interface.

Using the results of Fig. 5, we can now interpret the data of the Si 2p line shape as a function of layer thickness shown in Fig. 4. The Sr interface layer grown at 650 °C leaves the Si 2p unchanged. Therefore there is no evidence for the formation of silicide in the XPS spectra. Since oxidation of Sr and Ba took place at room temperature, silicide formation
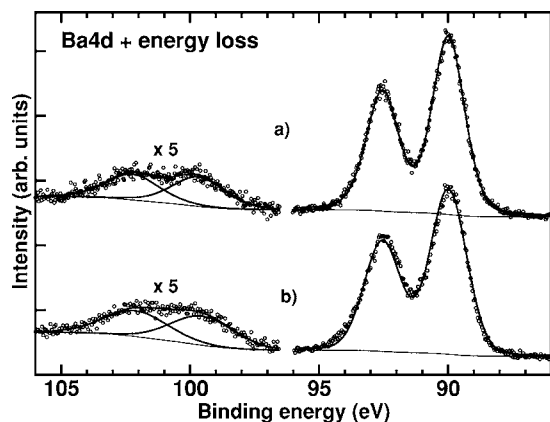
FIG. 5. XPS: Ba induced $4d_{5/2}$ and $4d_{3/2}$ peaks in oxide layers at 92.5 and 90.0 eV, respectively. A typical doublet of satellite peaks, shifted by ~9.7 eV with respect to the primary peaks is seen in the oxide. Examples are shown for (a) 62 ML of crystalline $Ba_{0.7}Sr_{0.3}O$ on Si(001), (b) 20 nm of amorphous $Sr_{0.3}Ba_{0.7}O$ on Ta. On the Si surface, the satellite peaks overlap with Si $2p$.

during the subsequent process is not possible either.

The initial step of oxidation forming mixed oxide layers is shown in the topmost graph of Fig. 4 on the left. The Si $2p$ emission shows a small satellite peak Si $2p$(II) at 101.4 eV binding energy, indicating that traces of SiO_x are formed. The shift by 1.7 eV with respect to the unoxidized Si $2p$ peak (I), however, is much smaller than for SiO_2, indicating that x must be $\leqslant 1$ and/or a mixed oxide with the Sr intermediate layer is formed.

For thicker layers, the Si $2p$ peaks (I) and (II) are damped, but two peaks indicated by the dashed line (right side of Fig. 4) grow relative to the unoxidized main peak with increasing oxide layer thickness. This behavior, however, does not indicate any increase of Si oxidation at the interface. As presented above, these peaks are exclusively due to the satellites of Ba $4d$. This was proven by determining the positions, shapes, and intensities of the Ba $4d$ satellites relative to the main Ba $4d$ peaks for a 62 ML thick $Ba_{0.7}Sr_{0.3}O$ layer. Taking these spectra as fixed, the satellite peaks were separated from the Si $2p$ peak and the interface oxide peak for each growth step, as shown in the left part of Fig. 4 by the dashed lines. This Ba satellite emission is the only emission remaining in the energy range of the Si $2p$ peaks for layer thicknesses above 10 nm.

The exponential damping of the Si $2p$ features as a function of oxide thickness, shown in the bottom panel of Fig. 7, is in agreement with these findings, and proves that no SiO_2 is formed during the oxidation process, while the interface remains sharp.

The O $1s$ emission shown in Fig. 6 is fully consistent with this scenario just described and reveals even more details. The initial growth of 1 ML of mixed oxide on the Sr interlayer yields three peaks in the O $1s$ spectrum. As clear from the spectra of thicker layers, the emission with the lowest binding energy at 529.8 eV, marked (I), is characteristic of the homogeneous $Ba_{0.7}Sr_{0.3}O$ layer. This peak shifts little from 1 to 6 ML thickness due to a deviating element ratio at the initial growth, caused by the Sr intermediate layer. The
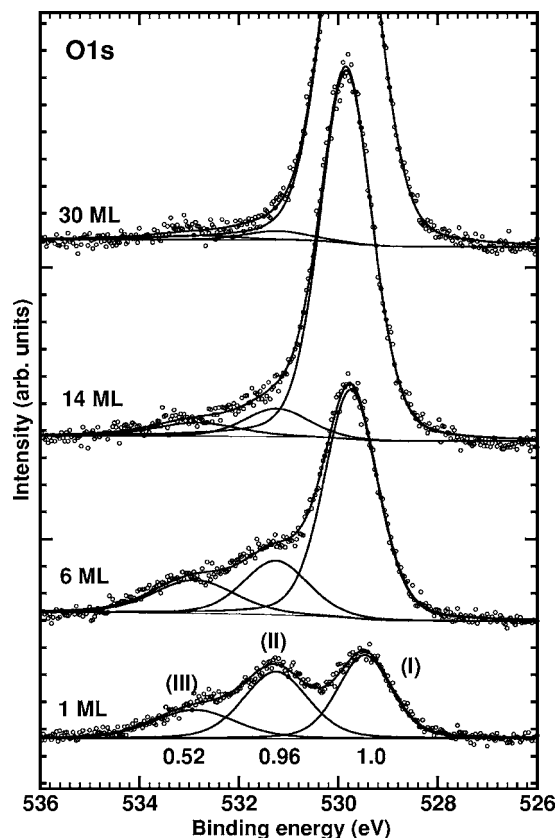

FIG. 6. O $1s$ XPS spectra at various stages of oxide growth. Peaks marked (II) and (III) are characteristic for the oxide layer formed at the interface to Si(100). As seen, they disappear gradually for thicker layers. Only peak (I) at 529.8 eV of the $Sr_{0.3}Ba_{0.7}O$ remains.

other two peaks, (II) at 531.5 and (III) at 533.1 eV, appear simultaneously and are due to species located at the interface to Si. O $1s$ peak (III) belongs to a mono-oxidized Si species, as already discussed above, and O $1s$ peak (II) to oxygen which is coordinated both with Sr and with Si.[24,25] For further quantitative analysis and for easy comparison we assign each O $1s$ peak at the initial growth an intensity relative to the intensity of the O $1s$ peak (I) of 1 ML oxygen in the first $Ba_{0.7}Sr_{0.3}O$ layer. These intensities are written below the bottom O $1s$ spectrum in Fig. 6. They allow us to determine the absolute oxygen amount at the interface within an uncertainty of about 20%. Both interface peaks are damped during the subsequent growth until they vanish in the noise. The damping characteristics as a function of layer thickness is shown in the top panel of Fig. 7. Both peaks are damped by the same factors, their ratio staying constant, as expected for an oxidic layer located at the interface. Therefore the oxidized interface layer remains unchanged during growth of thicker oxide layers, in agreement with the conclusions drawn from the Si $2p$ spectra. Again, there are no indications for further oxidation of Si during this process. These findings are fully compatible with the suggested oxidic interface layer,[10] where with 1.5 ML of oxygen at the interface two differently coordinated oxygen species are expected (see Sec. III C).
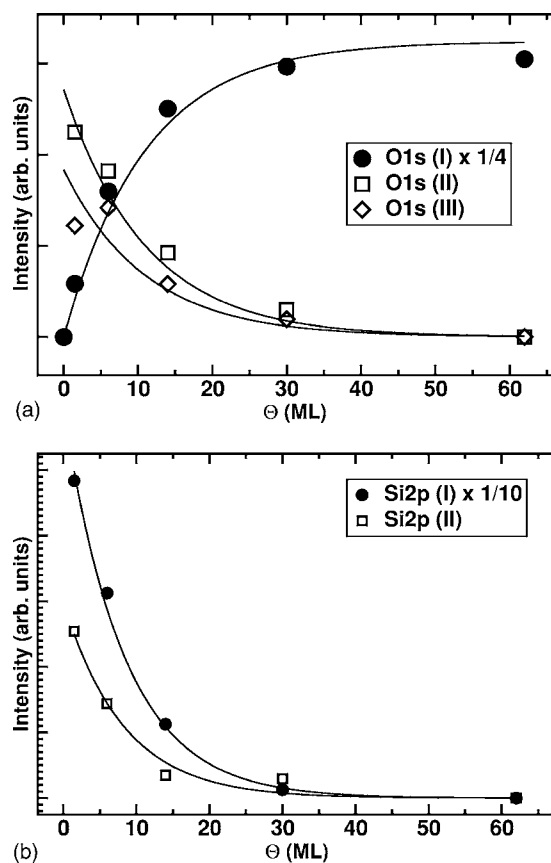
FIG. 7. Top: O 1s peaks as a function of oxide thickness. Assuming that the interface species ($\Diamond$, $\Box$) are localized in the first layer at the interface, damping of the interface peaks as a function of oxide thickness and the simultaneous increase of the oxide peak of $Sr_{0.3}Ba_{0.7}O$ can be well described, as the lines show. Bottom: Similar data for the Si 2p peaks of Si and of the SiO_x interface oxide. Si 2p and O 1s data sets are described by the same damping parameters, respectively.

To summarize this section, our spectroscopic data show that a mixed Sr–Si–O layer is formed at the interface, which has a thickness of at most 2 ML. This interface remains unchanged under our growth conditions, as well as after annealing up to 600 °C, as tested. Under the well controlled conditions of our experiments further oxidation of the Si interface during growth of the oxide layers turned out not to be a problem. No traces of SiO_2 were detectable in our spectra, nor did we find indications for silicide formation.

2. Band gap and excitonic structure

The size of the band gaps was investigated with EELS for 20 nm of pure amorphous SrO and BaO, and for a crystalline 30 ML (8.15 nm) thick $Sr_{0.3}Ba_{0.7}O$ layer. The results are plotted in Fig. 8 together with fits in order to determine the position of the excitonic loss and of the lowest interband excitation. For this purpose, the losses starting at energies above 3 eV were fitted by a model of the elastic peak consisting of three Gaussians, where the ratios between the peaks was fixed, but the overall intensity and the half-widths were free. This gave a very stable fit also for the loss peaks.
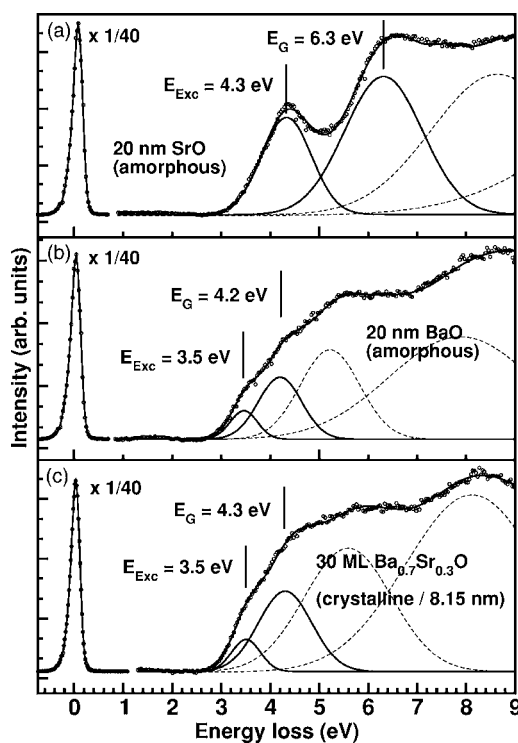

FIG. 8. Energy loss spectra of (a) 20 nm of amorphous SrO, (b) 20 nm of amorphous BaO, and (c) 30 ML (8.15 nm) of crystalline $Ba_{0.7}Sr_{0.3}O$. Full lines: Fits to the data using a set of Gaussian functions, as described in the text. Only the first two are shown that characterize the excitonic loss and the onset of valence band excitations, respectively. Primary energy 100 eV.

The lowest two peaks, assigned to the excitation of the lowest energy state of the exciton and to the lowest interband excitation, respectively, are plotted by continuous lines. Two of the additional peaks, which stabilize the fit, were plotted by dashed lines.

For SrO the exciton excitation at 4.3 eV is very well separated from the first interband excitation at 6.3 eV. This value corresponds very closely to the bulk values of cleaved single crystals also observed by EELS.[26] This peak structure, although not limited by the resolution of the instrument of about 0.2 eV, is so broad that surface and volume excitations cannot be separated. This is even more true for BaO, where we see a strong overlap between excitonic and band excitation. Nevertheless, the determination of the exciton excitation at 3.5 eV and the band gap of 4.2 eV is still possible, which is in reasonable agreement with other EELS measurements[26,27] and optical studies.[28,29] Interestingly, the mixed $Ba_{0.7}Sr_{0.3}O$ layer has a band gap only 0.1 eV higher, i.e., its value of 4.3 eV is mainly determined by the majority species in the oxide. The same is found for the excitonic excitation at 3.5 eV. A band gap of 5 eV of $Ba_{0.7}Sr_{0.3}O$ is quoted in literature,[7,8] unfortunately the cited publications[2,30] contain no information about the $Ba_{0.7}Sr_{0.3}O$ band gap.

Using identical fitting procedures, the band gap as a function of layer thickness was investigated for the $Ba_{0.7}Sr_{0.3}O$. As Fig. 9 shows, there is a complete independence of the size of the band gap on layer thickness. This is even true for the thinnest layer of 1 ML, and may indicate that initial growth
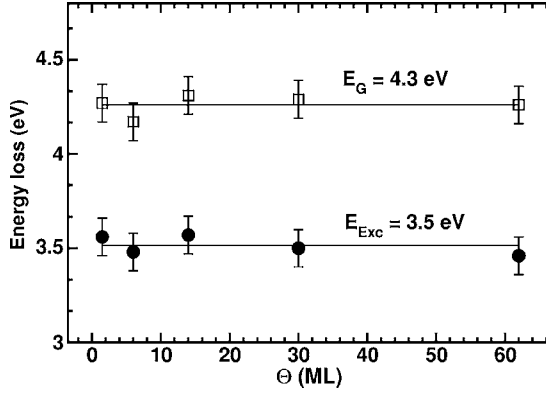
FIG. 9. Energetic position of the excitonic loss and width of the band gap as a function of layer thickness of $Ba_{0.7}Sr_{0.3}O$, determined by fits as in Fig. 8.

proceeds by (at least) double layer formation. The same constancy as a function of layer thickness was found for the exciton excitation. These results, however, are not uncommon for insulating material without surface states in the band gap and corresponding small relaxations at the surface.[31,32]

3. Band discontinuity

Valence band discontinuities were measured following the method of Waldrop $et\ al.$[33] This method was also used successfully to determine as schematically the band discontinuities of silicon/insulator heterojunctions.[34,35] The method is based on x-ray photoemission measurements of the energetic distance of arbitrary core lines and valence band edges of bulk materials of the silicon substrate and of the insulator adsorbate, and the energetic distance of the same core lines for the silicon/insulator heterojunctions, as schematicly shown in Fig. 10. To find the valence band edge E_v, the linear portion of the valence band leading edge was extrapolated to the flat energy distribution curve in the energy gap, as shown in Fig. 11. The intercept was defined as E_v. The valence band offset for clean n-Si(001) was determined as 0.6 ± 0.1 eV, in reasonable agreement with the value determined by Mönch $et\ al.$[36] (0.56 ± 0.02 eV). For the n
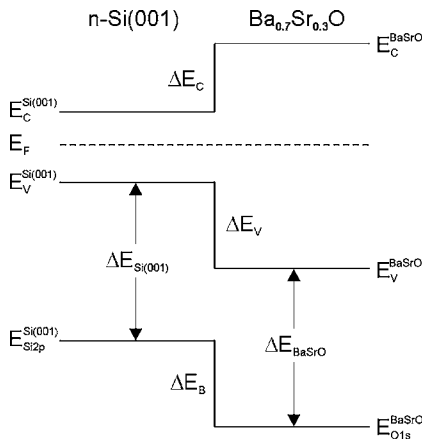

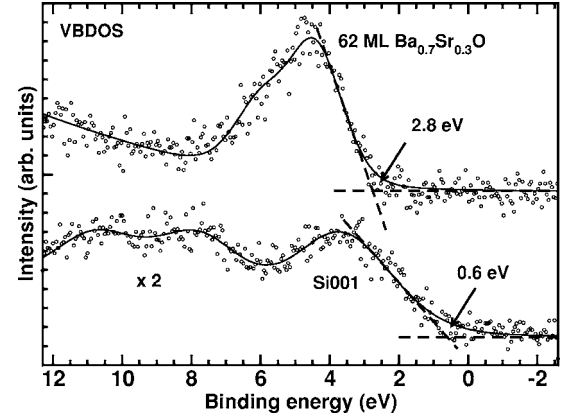FIG. 10. Schematic energy band diagram of an abrupt $Sr_{0.3}Ba_{0.7}O/n$-Si(001) heterojunction interface.

FIG. 11. Valence band photoelectron spectra for n-Si(001) and for a 62 ML ($\sim$17 nm) thick $Ba_{0.7}Sr_{0.3}O$ layer on Si(001).

-Si(001) substrate the energetic distance between the Si $2p$ line and the valence band edge was measured to be $\Delta E_{Si(001)} = (E_{Si\ 2p}^{Si(001)} - E_v^{Si(001)}) = 99.1 \pm 0.1$ eV. Due to the lack of $Ba_{0.7}Sr_{0.3}O$ bulk material, we used a 62 ML (16.8 nm) thick $Ba_{0.7}Sr_{0.3}O$ layer on Si(001) instead of bulk material. The leading edge of the valence band for 62 ML $Ba_{0.7}Sr_{0.3}O$ was found as 2.8 ± 0.1 eV, the energetic distance between the O $1s$(I) line (see Fig. 6) and the valence band edge to be $\Delta E_{BaSrO} = (E_{O\ 1s(I)}^{62\ ML\ BaSrO} - E_v^{62\ ML\ BaSrO}) = 526.9 \pm 0.1$ eV. The energetic distance between the O $1s$(I) line and the Si $2p$(I) line
(see Fig. 4) was measured for a heterojunction of 6 ML
(16.3 A) $Ba_{0.7}Sr_{0.3'}O$ to be $\Delta E_B = (E_{O\ 1s(I)}^{6\ ML\ BaSrO} - E_{Si\ 2p(I)}^{6\ ML\ BaSrO})$
$= 430.02 \pm 0.05$ eV. The valence band discontinuities are now calculated as follows:

$$\Delta E_B + \Delta E_{Si(001)} - \Delta E_{BaSrO} = 2.2 \pm 0.1 \text{ eV}.$$

Then, from the known band gaps of Si (1.12 eV) and of $Ba_{0.7}Sr_{0.3}O$ (4.3 eV) a conduction band offset of 1.0 ± 0.1 eV is found. The small shift of the Si $2p$ line to higher binding energy suggests a small reduction of band bending induced by the $Ba_{0.7}Sr_{0.3}O$ adsorbate of $(E_{Si\ 2p(I)}^{6\ ML} - E_{Si\ 2p}^{Si(001)})$ $= 0.09 \pm 0.05$ eV. Since this is within the error of the position of the leading edges of the valence band, the simple difference between the valence band edges of $(E_v^{62\ ML\ BaSrO} - E_v^{Si(001)}) = 2.2 \pm 0.1$ eV also reflects the valence band discontinuity within the given accuracy. Figure 12 summarizes the band discontinuity and band bending at the $Ba_{0.7}Sr_{0.3}O/n$-Si(001) heterojunction. Since the heterojunction depletion layer is larger than the electron escape depth, the measured band discontinuity is not affected by band bending. The band bending of the clean n-Si(001) surface of -0.54 ± 0.01 eV[36] is decreased by 0.09 ± 0.05 eV to -0.45 ± 0.05 for the heterojunction, but remains in the range of depletion.

C. Interface structure

To understand the structure of the interface presented in Sec. III B 1, we directly oxidized Sr coverages of 1/3 and 1.2 ML on the Si(001) surface. The resulting O $1s$ spectra
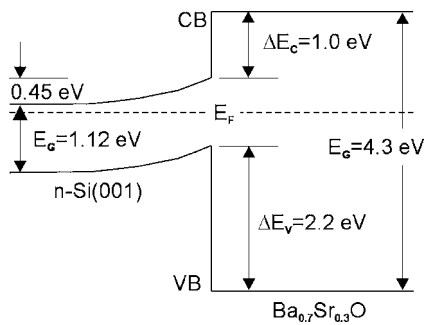
FIG. 12. Energy level diagram for the $Sr_{0.3}Ba_{0.7}O/n$-Si(001) heterojunction.

and SPA-LEED line scans are shown in Figs. 13 and 14, respectively. The scale of the O $1s$ spectra is the same, for easy comparison.

An amount of 1/3 ML Sr evaporated at 820 °C onto the Si(001) substrate results in a (3×2) reconstruction.[14] In a first step, we oxidized the (3×2)-reconstructed surface for 2 min at a substrate temperature of 480 °C and at a pressure of 2×10^{-7} mbar O_2, which corresponds to an exposure of 18 L [1 L (Langmuir)$= 10^{-6}$ torr s]. The former (3×2) reconstruction was converted into a (2×1) reconstruction with weak spots at third order positions, as shown in the bottom inset of Fig. 13. Two peaks already known from Sec. III B 1 were observed in the O $1s$ spectrum. According to the assignment made there, the left peak (III) belongs to the Si−O bonds, peak (II) to Sr−O−Si bonds. In a second step we
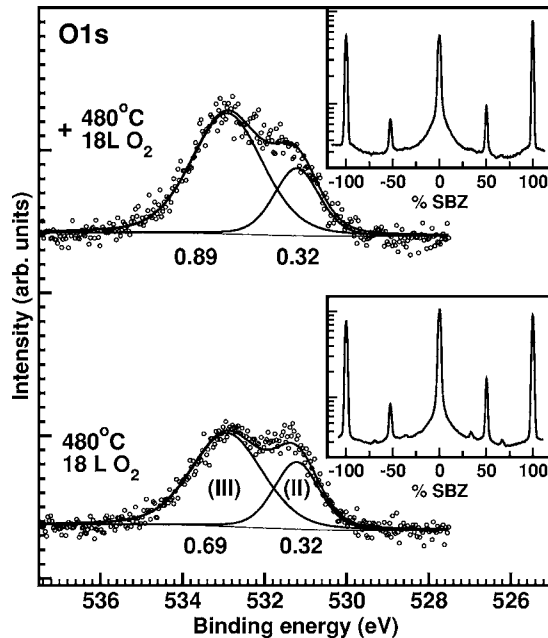

FIG. 13. O $1s$ spectra of an oxidized 1/3 ML thick Sr layer on Si(001). Bottom: first oxidation step at 480 °C, oxygen exposure 18 L. Top: second oxidation step again at 480 °C with the same amount of oxygen added. SPA-LEED line scans through (01), (00), and (0$\bar{1}$) beams after each oxidation step are shown in the insets. XPS intensities relative to the O $1s$ peak of 1 ML $Ba_{0.7}Sr_{0.3}O$ are marked below each peak.
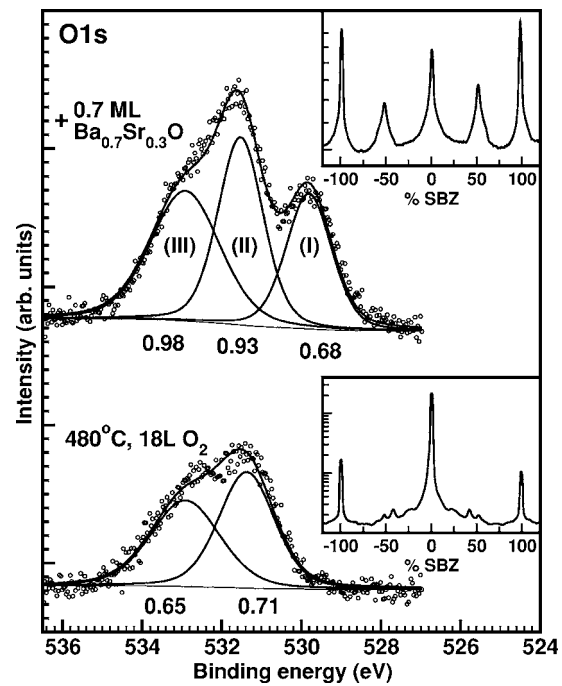

FIG. 14. Bottom: O $1s$ spectrum of a 1.2 ML thick Sr layer, oxidized at 480 °C with 18 L of oxygen, on Si(100). Top: 0.7 ML $Ba_{0.7}Sr_{0.3}O$ grown on top of the partly oxidized Sr layer. SPA-LEED line scans (same sections as in Fig. 13) are shown in the insets. Intensities relative to the O $1s$ peak of 1 ML $Ba_{0.7}Sr_{0.3}O$ are marked again below each peak.

oxidized this layer again at 480 °C with additional 18 L. The weak spots at third order position almost disappeared, and only a (2×1) reconstruction remained. In the O $1s$ spectrum peak (III) increased by one-third, whereas peak (II) remained unchanged, as shown in the top of Fig. 13. Comparing the relative intensities of the O $1s$ peak (III) with the O $1s$ peak (I) of 1 ML $Sr_{0.3}Ba_{0.7}O$ in Fig. 6 the second oxidation step forms a coverage of nearly 1 ML of oxygen in Si−O bonds at the surface. The Sr was already oxidized completely at the first oxidation step, and contains 1/3 ML of oxygen in Sr−O−Si bonds. This confirmed the calibration of 1 ML oxygen in Fig. 6.

As already presented in Fig. 1, an amount of 1.2 ML Sr evaporated at 650 °C onto Si(001) forms a (5×1) reconstruction. The result of the oxidation of such a (5×1) reconstructed surface at 480 °C and 18 L is presented in the bottom part of Fig. 14. LEED shows a (1×1) reconstruction with weak spots at half and fifth order positions. The O $1s$ spectrum splits again into the two known peaks, but the intensities of both peaks indicate that only partial oxidation has taken place. By evaporating an amount of 0.7 ML $Sr_{0.3}Ba_{0.7}O$ at RT on top of this partially oxidized Sr layer, the intensities of O $1s$ peaks (I) and (II) increase. Both now reach an intensity equivalent to roughly 1 ML, according to our calibration, as shown in the upper part of Fig. 14, due to the catalytic action of Ba on the oxidation. The line scan in the upper inset in Fig. 14 now shows a broadened (2×1) reconstruction. Further growth of $Sr_{0.3}Ba_{0.7}O$ onto this layer results again in the (1×1) alignment, but with a significantly

lower crystalline quality than without prior oxidation of the interface.

We note that the intensity of the O 1s peak (III) in the spectrum in the upper part of Fig. 14 is significantly higher than in the spectrum of 1 ML $Ba_{0.7}Sr_{0.3}O$ in Fig. 6, indicating less oxygen directly coordinated with Si in this layer. Even taking into account the slight increase of this peak during multilayer growth (see upper graph of Fig. 7), peak (III) reaches only 70% of peak (II) during direct oxide growth on the Sr(5×1) layer without the intermediate step of complete interface oxidation. Therefore this interface contains not more than 0.7 ML of oxygen coordinated in Si–O bonds and 1 ML of oxygen coordinated in Sr–O–Si bonds. A similar behavior of the oxidation of Sr coverages of 1/3 and 1/2 ML on Si(001) is described in Ref. 24.

The Si 2p spectra of the different oxidation and growth steps offer no further information. The behavior is equivalent to that shown in Fig. 4. The intensity of Si 2p peak (II) scales with the intensity of O 1s peak (III), whereas the position remains unchanged. The distance of 1.7 eV to the Si 2p main peak primary indicates SiO.

The different electronic environments of oxygen ions at the interface, which for the coordination with Sr atoms find their expression by the O 1s peak (I) and (II), are also seen in the shift of the Sr3d (not shown here) during the different oxidation and growth steps. The oxidation of the first Sr layer results in a broadening of about 20% and a small shift of the $Sr3d_{3/2}$ peak to lower binding energy by about 0.2 eV induced by the formation of Sr–O–Si bonds. Further growth of 1 ML $Ba_{0.7}Sr_{0.3}O$ or more gives rise to a further shift of about -0.6 eV due to the higher ionicity of Sr in the $Ba_{0.7}Sr_{0.3}O$.

IV. DISCUSSION AND SUMMARY

From our results we obtain the following description of the interface between the Si(001) surface and the $Ba_{0.7}Sr_{0.3}O$ layer: Our deposition procedure leads to an abrupt interface between Si and the mixed oxide that extends over not more than the two topmost Si layers and one layer of Sr. This follows from the saturation of oxidation at integer values of monolayers. This interface contains up to 2 ML of oxygen, which is distributed in the following way: The Sr layer as the starting interface layer is oxidized completely into Sr—O—Si bonds, containing 1 ML of oxygen. In addition, up to 1 ML oxygen is located in Si–O bonds. No traces of SiO_2 were found. This fully oxidized interface, however, is not best suited for growth of crystalline mixed oxides. Indeed, a reduced oxygen content of 1.5 to 1.7 ML at the interface seems to be more favorable for the subsequent growth of a crystalline $Ba_{0.7}Sr_{0.3}O$ layer.

As a signature for the oxidized Sr layers as well as of complete interfaces, we find a (2×1) reconstruction. This is in full agreement with the results of density functional theory calculations of SrO interfaces presented by Först *et al.*[10] They find (2×1)-reconstructed SrO interfaces consisting of 1/2 ML of Sr and of 1 to 1.5 ML of oxygen. At a coverage of 1/2 ML of Sr, the strontium atoms first occupy the troughs between the dimer rows in the center of four dimers, resulting in the (2×1) reconstruction. In order to be compatible with our findings with 1 ML Sr in the interface, the strontium atoms must also occupy locations between two dimers. Since these sites are not equivalent, still a (2×1) reconstruction can be maintained. The subsequently deposited $Ba_{0.7}Sr_{0.3}O$ layer seems to level off this modulation of the substrate.

Our low temperature procedure to grow lattice-matched crystalline $Ba_{0.7}Sr_{0.3}O$ on the Si(001) substrate demonstrates the feasibility of an alternative process to that described in previous studies.[2,6–9] In our oxidation process of the interface at low temperatures we were not able to identify spectroscopically any species that may be called a silicide. Instead, all Sr atoms at the interface are completely oxidized. This is again in agreement with the findings of Ref. 10. We note that for oxidized Sr layers our spectroscopic data agree rather well with those of Ref. 24, but the notation as a silicate species seems to be inappropriate because all species at the interface are still in a two-dimensional layer, for which the local coordination differs strongly from that of bulk silicate phases, as does the lattice constant. Our results are partly corroborated by previous publications[24,37] that found indications that silicides at the interface are not stable during oxidation. This must be even more true at elevated temperatures.

Summarizing, $Ba_{0.7}Sr_{0.3}O$ grows crystalline and lattice matched on the Si(001) surface. The interface discussed above forms an abrupt heterojunction between the substrate and the oxide. The combination of a band gap of 4.3 eV, a band offset with respect to *n*-Si of -2.2 eV, and a conduction band offset of $+1.0$ eV shows that this system is a promising candidate for alternative gate oxides. As suggested recently,[10] it might be possible to tune the band gap as well as band alignment in such materials by manipulating the interface.

*Electronic address: pfnuer@fkp.uni-hannover.de

[1] K. Hubbard and D. Schlom, J. Mater. Res. **11**, 2757 (1996).

[2] R. A. McKee, F. J. Walker, and M. F. Chisholm, Phys. Rev. Lett. **81**, 3014 (1998).

[3] B. K. Moon and H. Ishiwara, Jpn. J. Appl. Phys., Part 1 **33**, 1472 (1994).

[4] O. Nakagawara, M. Kobayashi, Y. Yoshino, Y. Katayama, H. Tabata, and T. Kawai, J. Appl. Phys. **78**, 7226 (1995).

[5] H. Mori and H. Ishiwara, Jpn. J. Appl. Phys., Part 1 **30**, 1415 (1991).

[6] R. A. McKee, F. J. Walker, J. R. Conner, E. D. Specht, and D. E. Zelmon, Appl. Phys. Lett. **59**, 782 (1991).

[7] R. A. McKee, F. J. Walker, and M. F. Chisholm, Sci. Mag. **293**, 468 (2001).

[8] R. A. McKee, F. J. Walker, M. B. Nardelli, W. A. Shelton, and G. M. Stocks, Sci. Mag. **300**, 1726 (2003).

[9] M. B. Nardelli, F. J. Walker, and R. A. McKee, Phys. Status Solidi B **241**, 2279 (2004).

[10] C. Först, C. Ashman, K. Schwarz, and P. Blöchl, Nature (London) **427**, 53 (2003).

[11] C. R. Ashman, C. J. Först, K. Schwarz, and P. E. Blöchl, Phys. Rev. B **69**, 075309 (2004).

[12] J. Lettieri, J. H. Haeni, and D. G. Schlom, J. Vac. Sci. Technol. A **20**, 1332 (2002).

[13] A. M. Stoneham and J. Dhote, *A Compilation of Crystal Data for Halides and Oxides* (2002), available online from www.cmmp.ucl.ac.uk/~ahh/research/crystal/homepage.htm, and references contained therein.

[14] W. C. Fan, N. J. Wu, and A. Ignatiev, Phys. Rev. B **42**, 1254 (1990).

[15] W. C. Fan and A. Ignatiev, Surf. Sci. **253**, 297 (1991).

[16] P. Blöchl (private communication).

[17] S. Dushman, *Scientific Foundations of Vacuum Technique* (Wiley, New York, 1949).

[18] W. C. Fan and A. Ignatiev, Phys. Rev. B **44**, 3110 (1991).

[19] W. C. Fan, A. Mesarwi, and A. Ignatiev, J. Vac. Sci. Technol. A **8**, 4017 (1990).

[20] A. Mesarwi and A. Ignatiev, J. Vac. Sci. Technol. A **9**, 2264 (1991).

[21] B. Hellsing, Phys. Rev. B **40**, 3855 (1989).

[22] C. Schwennicke, J. Schimmelpfennig, and H. Pfnür, Surf. Sci. **293**, 57 (1993).

[23] J. Zachariae and H. Pfnür (unpublished).

[24] Y. Liang, S. Gan, and M. Engelhard, Appl. Phys. Lett. **79**, 3591 (2001).

[25] P. D. Kirsch and J. G. Ekerdta, J. Vac. Sci. Technol. A **19**, 2222 (2001).

[26] A. R. Protheroe, A. Steinbrunn, and T. E. Gallon, Surf. Sci. **126**, 534 (1983).

[27] R. E. Thomas, A. Shih, and G. A. Haas, Surf. Sci. **75**, 239 (1978).

[28] R. J. Zollweg, Phys. Rev. **97**, 288 (1955).

[29] F. C. Jahoda, Phys. Rev. **107**, 1261 (1957).

[30] G. E. Jellison, Jr., L. A. Boatner, D. H. Lowndes, R. A. McKee, and M. Godbole, Appl. Opt. **33**, 6053 (1994).

[31] V. Henrich and P. Cox, *The Surface Science of Metal Oxides* (Cambridge University Press, Cambridge, England, 1996).

[32] V. Zielasek, T. Hildebrandt, and M. Henzler, Phys. Rev. B **62**, 2912 (2000).

[33] J. Waldrop, R. Grant, S. Kowalczyk, and E. Kraut, J. Vac. Sci. Technol. A **3**, 835 (1985).

[34] H. Osten, J. Liu, and H. Müssig, Appl. Phys. Lett. **80**, 297 (2002).

[35] S. Chambers, Y. Liang, Z. Yu, R. Droopad, J. Ramdani, and K. Eisenbeiser, Appl. Phys. Lett. **77**, 1662 (2000).

[36] W. Mönch, P. Koke, and S. Krueger, J. Vac. Sci. Technol. **19**, 313 (1981).

[37] D. P. Norton, C. Park, Y. E. Lee, and J. D. Budai, J. Vac. Sci. Technol. B **20**, 257 (2002).